REPORT DOCUMENTATION PAGE

Form Approved OMB NO. 0704-0188

1. REPORT DATE (DD-MM-YYYY)	2. REPORT TYPE	3. DATES COVERED (From - To)
17-01-2015	Final Report	17-Oct-2011 - 16-Oct-2014

4. TITLE AND SUBTITLE
Concept Validation and Optimization for a Vent-Based Mine-Blast Mitigation System

5a. CONTRACT NUMBER
W911NF-11-1-0518

5b. GRANT NUMBER

5c. PROGRAM ELEMENT NUMBER
611102

6. AUTHORS
Mica Grujicic

5d. PROJECT NUMBER

5e. TASK NUMBER

5f. WORK UNIT NUMBER

7. PERFORMING ORGANIZATION NAMES AND ADDRESSES
Clemson University
300 Brackett Hall

Clemson, SC 29634 -5702

8. PERFORMING ORGANIZATION REPORT NUMBER

9. SPONSORING/MONITORING AGENCY NAME(S) AND ADDRESS (ES)
U.S. Army Research Office
P.O. Box 12211
Research Triangle Park, NC 27709-2211

10. SPONSOR/MONITOR'S ACRONYM(S)
ARO

11. SPONSOR/MONITOR'S REPORT NUMBER(S)
60050-EG.25

12. DISTRIBUTION AVAILIBILITY STATEMENT
Approved for Public Release; Distribution Unlimited

13. SUPPLEMENTARY NOTES
The views, opinions and/or findings contained in this report are those of the author(s) and should not contrued as an official Department of the Army position, policy or decision, unless so designated by other documentation.

14. ABSTRACT
In this project, a new solution for improving blast-survivability of light tactical military vehicles to detonation of a shallow-buried mine underneath them has been introduced and analyzed computationally. The solution involves the use of side-vent-channels attached to the V-shaped vehicle underbody, and tries to exploit detonation-products' ultrasonic-expansion and ejected-soil venting phenomena to generate a downward thrust on the targeted vehicle. In order to accurately account for the interaction of detonation products, ejected soil and blast waves with the target structure, a novel combined Eulerian/Lagrangian finite-element/discrete-particle computational method has been

15. SUBJECT TERMS
Blast-mitigation; Vent-based concept; Fluid-structure interaction

16. SECURITY CLASSIFICATION OF:			17. LIMITATION OF ABSTRACT	15. NUMBER OF PAGES	19a. NAME OF RESPONSIBLE PERSON
a. REPORT	b. ABSTRACT	c. THIS PAGE			Mica Grujicic
UU	UU	UU	UU		19b. TELEPHONE NUMBER 864-656-5639

Report Title

Concept Validation and Optimization for a Vent-Based Mine-Blast Mitigation System

ABSTRACT

In this project, a new solution for improving blast-survivability of light tactical military vehicles to detonation of a shallow-buried mine underneath them has been introduced and analyzed computationally. The solution involves the use of side-vent-channels attached to the V-shaped vehicle underbody, and tries to exploit detonation-products' ultrasonic-expansion and ejected-soil venting phenomena to generate a downward thrust on the targeted vehicle. In order to accurately account for the interaction of detonation products, ejected soil and blast waves with the target structure, a novel combined Eulerian/Lagrangian finite-element/discrete-particle computational method has been developed and employed. To assess the full blast-mitigation potential of the new concept, the finite-element-based analysis has been combined with an advanced multi-objective design-optimization procedure. The results obtained show that the proposed concept has a relatively limited (but respectable) ability to reduce the detonation-induced total momentum transferred to, and the acceleration acquired by, the target vehicle.

Enter List of papers submitted or published that acknowledge ARO support from the start of the project to the date of this printing. List the papers, including journal references, in the following categories:

(a) Papers published in peer-reviewed journals (N/A for none)

Received		Paper
04/27/2012	1.00	M. Grujicic, B. Pandurangan, A. Hariharan. Comparative Discrete-Particle Versus Continuum-Based Computational Investigation of Soil Response to Impulse Loading, Journal of Materials Engineering and Performance, (11 2011): 1520. doi: 10.1007/s11665-011-9844-0
06/24/2013	4.00	Mica Grujicic, B. Pandurangan, W. C. Bell, S. Bagheri. Shock-Wave Attenuation and Energy-Dissipation Potential of Granular Materials, Journal of Materials Engineering and Performance, (5 2011): 0. doi: 10.1007/s11665-011-9954-8
06/24/2013	13.00	M. Grujicic, J.S. Snipes , N. Chandrasekharan. Fluid-structure interaction computational analysis of a piston-cylinder based blast-wave-mitigation concept, Multidiscipline Modeling in Materials and Structures, (10 2012): 524. doi: 10.1108/15736101211281632
06/24/2013	8.00	. Computational Investigation of Blast-wave-mitigation via the Use of Air-vacated Buffers, Journal of Modern Mathematics Frontier, (11 2012): 28. doi:
06/24/2013	7.00	M. Grujicic, R. Yavari, J. S. Snipes, S. Ramaswami. Extension of a Current Continuum-Level Material Model for Soil into the Low-Density Discrete-Particle Regime, Journal of Materials Engineering and Performance, (11 2012): 0. doi: 10.1007/s11665-012-0429-3
06/24/2013	6.00	M. Grujicic, J. Snipes, N. Chandrasekharan. Computational analysis of fluid-structure interaction based blast-mitigation effects, Proceedings of the Institution of Mechanical Engineers, Part L: Journal of Materials: Design and Applications, (01 2013): 0. doi: 10.1177/1464420712470356
07/25/2014	22.00	M. Grujicic , B. d'Entremont , J. S. Snipes, R. Gupta . A Novel Blast-mitigation Concept for Light Tactical Vehicles, ARL Technical Report ARL-TR-6735, (11 2013): 1. doi:
07/25/2014	23.00	M. Grujicic, R. Yavari, J. S. Snipes, S.Ramaswami, R. Gupta. A Combined Finite-Element/Discrete-Particle Analysis of a Side-Vent-Channel-Based Concept for Improved Blast-Survivability of Light Tactical Vehicles, ARL Technical Report ARL-TR-6736, (11 2013): 1. doi:
07/30/2014	21.00	J.S. Snipes, N. Chandrasekharan, M. Grujicic, S. Ramaswami. Computational assessment of the blast-mitigation efficacy of an air-vacated protective-buffer concept, Multidiscipline Modeling in Materials and Structures, (04 2013): 218. doi: 10.1108/MMMS-04-2013-0029
TOTAL:		**9**

Number of Papers published in peer-reviewed journals:

(b) Papers published in non-peer-reviewed journals (N/A for none)

Received Paper

TOTAL:

Number of Papers published in non peer-reviewed journals:

(c) Presentations

Number of Presentations: 0.00

Non Peer-Reviewed Conference Proceeding publications (other than abstracts):

Received Paper

TOTAL:

Number of Non Peer-Reviewed Conference Proceeding publications (other than abstracts):

Peer-Reviewed Conference Proceeding publications (other than abstracts):

Received Paper

TOTAL:

Number of Peer-Reviewed Conference Proceeding publications (other than abstracts):

(d) Manuscripts

Received	Paper	
03/20/2014	18.00	M. Grujicic, R. Yavari, J. S. Snipes, S.Ramaswami, R. Gupta. COMPUTATIONAL ANALYSIS OF SIDE-VENT-CHANNELS SOLUTION FOR IMPROVING SURVIVABILITY OF LIGHT-TACTICAL-VEHICLE SUBJECTED TO SHALLOW-BURIED UNDERBODY MINE DETONATION , ARL Technical Report (12 2013)
03/20/2014	19.00	M. Grujicic, R. Yavari, S.Ramaswami, J. S. Snipes, R. Gupta. SHAPE/SIZE OPTIMIZATION OF SIDE-VENT-CHANNELS SOLUTION FOR IMPROVED LIGHT-TACTICAL-VEHICLE SURVIVABILITY TO BENEATH-UNDERBODY SHALLOW-BURIED MINE DETONATION , ARL Technical Report (09 2013)
04/27/2012	2.00	M. Grujicic, B. d'Entremont, J. S. Snipes, R. Gupta. A Novel Blast-mitigation Concept for Light Tactical Vehicles, Depending on the decision by the ARL, the manuscript will be published either internally or in International Journal of Impact Engineering (04 2012)
05/15/2014	20.00	M. Grujicic, R. Yavari, J. S. Snipes, S. Ramaswami, R. Gupta. Improvements in the Blast-Mitigation Performance of Light-Tactical-Vehicle Side-Vent-Channel Solution using Aluminum-Foam Core Sandwich Structures, Manuscript (05 2014)
06/24/2013	9.00	M. Grujicic , B. d'Entremont , J. S. Snipes, R. Gupta. A NOVEL BLAST-MITIGATION CONCEPT FOR LIGHT TACTICAL VEHICLES , ARL Technical Report (03 2013)
06/24/2013	12.00	M. Grujicic , J. S. Snipes , N. Chandrasekharan , S. Ramaswami. COMPUTATIONAL ASSESSMENT OF THE BLAST-MITIGATION EFFICACYOF AN AIR-VACATED PROTECTIVE-BUFFER CONCEPT, Multidiscipline Modeling in Materials and Structures (04 2013)
06/24/2013	11.00	M. Grujicic , R. Yavari , S.Ramaswami , J. S. Snipes, R. Gupta. SHAPE/SIZE OPTIMIZATION OF SIDE-VENT-CHANNELS SOLUTIONFOR IMPROVED LIGHT-TACTICAL-VEHICLE SURVIVABILITY TO BENEATH-UNDERBODY SHALLOW-BURIED MINE DETONATION , ARL Technical Report (06 2013)
06/24/2013	10.00	M. Grujicic , R. Yavari , J. S. Snipes , S.Ramaswami, R. Gupta. A COMBINED FINITE-ELEMENT/DISCRETE-PARTICLE ANALYSIS OF A SIDE-VENT-CHANNEL-BASED CONCEPT FOR IMPROVED BLAST-SURVIVABILITY OF LIGHT TACTICAL VEHICLES, ARL Technical Report (05 2013)
07/02/2012	3.00	M. Grujicic , J. S. Snipes , N. Chandrasekharan . FLUID-STRUCTURE INTERACTION COMPUTATIONAL ANALYSIS OF A PISTON-CYLINDER BASED BLAST-WAVE-MITIGATION CONCEPT, Multidiscipline Modeling in Materials and Structures (02 2012)
07/02/2013	16.00	M. Grujicic, B. d'Entremont, J. S. Snipes, R. Gupta. Side-vent-channel-based Novel Blast-mitigation Concept for Light Tactical Vehicles, ARL Technical Report (06 2013)
07/02/2013	14.00	M. Grujicic , B. Pandurangan , W. C. Bell , S. Bagheri. Shock-Wave Attenuation/Dispersion Potential of Granular Materials, Journal of Materials Engineering and Performance (06 2013)

07/02/2013 15.00 M. Grujicic , J. S. Snipes , N. Chandrasekharan , R. Gupta. Piston-Cylinder Based Blast-Wave-Mitigation Concept: A Fluid-Structure Interaction Computational Analysis, Multidiscipline Modeling in Materials and Structures (06 2013)

08/23/2013 17.00 M. Grujicic, R. Yavari, J. S. Snipes, S.Ramaswami, R. Gupta. COMPUTATIONAL ANALYSIS OF SIDE-VENT-CHANNELS SOLUTION FOR IMPROVED LIGHT-TACTICAL-VEHICLE SURVIVABILITY TO BENEATH-UNDERBODY SHALLOW-BURIED MINE DETONATION , ARL Technical Report (08 2013)

10/09/2014 24.00 M. Grujicic, R. Yavari , J. S. Snipes , S. Ramaswami , R. Gupta. MITIGATION OF BLAST AND IMPACT LOADING VIA THE USE OFA ZEOLITE-ABSORBENT/NANO-FLUIDICS PROTECTION SYSTEM, International Journal of Structural Integrity (09 2014)

TOTAL: **14**

Number of Manuscripts:

Books

Received Book

TOTAL:

Received Book Chapter

TOTAL:

Patents Submitted

Patents Awarded

Awards

1. Eastman Chemical Faculty Excellence Award, 2012.

2. 2012 SAGE Best Paper Award
M Grujicic, W. C. Bell, B. Pandurangan, B. A. Cheeseman, C. Fountzoulas, P. Patel, D. W. Templeton, and K. D. Bishnoi, "The effect of high-pressure densification on ballistic-penetration resistance of a soda-lime glass", Journal of Materials: Design and Applications, 225(4), pp. 298-315, 2011.

3. Emerald Publishing Literati Network Awards for Excellence 2011
M. Grujicic, H. Marvi, G. Arakere, W. C. Bell, I. Haque, "The Effect of Up-armoring the High-Mobility Multi-purpose Wheeled Vehicle (HMMWV) on the Off-road Vehicle Performance," Multidiscipline Modeling in Materials and Structures, 6(2), 2010, 229-256.

4. Alumni Award for Outstanding Achievement in Research, April 2011

5. 2009 PE Publishing Prize
M. Grujicic, T. He, B. Pandurangan, W. C. Bell, N. Coutris, B. A. Cheeseman, W. N.Roy and R. R. Skaggs, "Development, Parameterization and Validation of a Visco-Plastic Material Model for Sand With Different Levels of Water Saturation", Journal of Materials: Design and Applications, 223, pp. 63-81, 2009

Graduate Students

NAME	PERCENT_SUPPORTED	Discipline
Ramin Yavari	0.25	
Rohan Galgalikar	0.25	
Varun Chenna	0.25	
Vasudeva Avuthu	0.25	
FTE Equivalent:	**1.00**	
Total Number:	**4**	

Names of Post Doctorates

NAME	PERCENT_SUPPORTED
Jennifer Snipes	0.50
Subrahmanian Ramaswami	0.50
FTE Equivalent:	**1.00**
Total Number:	**2**

Names of Faculty Supported

NAME	PERCENT_SUPPORTED	National Academy Member
Mica Grujicic	0.10	
FTE Equivalent:	**0.10**	
Total Number:	**1**	

Names of Under Graduate students supported

NAME	PERCENT_SUPPORTED
FTE Equivalent:	
Total Number:	

Student Metrics

This section only applies to graduating undergraduates supported by this agreement in this reporting period

The number of undergraduates funded by this agreement who graduated during this period: 0.00

The number of undergraduates funded by this agreement who graduated during this period with a degree in science, mathematics, engineering, or technology fields:..... 0.00

The number of undergraduates funded by your agreement who graduated during this period and will continue to pursue a graduate or Ph.D. degree in science, mathematics, engineering, or technology fields:..... 0.00

Number of graduating undergraduates who achieved a 3.5 GPA to 4.0 (4.0 max scale):..... 0.00

Number of graduating undergraduates funded by a DoD funded Center of Excellence grant for Education, Research and Engineering:..... 0.00

The number of undergraduates funded by your agreement who graduated during this period and intend to work for the Department of Defense 0.00

The number of undergraduates funded by your agreement who graduated during this period and will receive scholarships or fellowships for further studies in science, mathematics, engineering or technology fields: 0.00

Names of Personnel receiving masters degrees

NAME
Ramin Yavari
Varun Chenna
Total Number: **2**

Names of personnel receiving PHDs

NAME
Total Number:

Names of other research staff

NAME	PERCENT_SUPPORTED
FTE Equivalent:	
Total Number:	

Sub Contractors (DD882)

Inventions (DD882)

Scientific Progress

See attachment.

Technology Transfer

The fluid-structure interaction model development efforts have been carried out in close collaboration with the researchers from the Army Research Laboratory, Aberdeen Proving Ground. This collaboration includes transfer of the fluid-structure interaction user subroutines to the Army Research Laboratory collaborator (Dr. Rahul Gupta) for further testing and validation.

Project Title:

Concept Validation and Optimization

for a Vent-Based Mine-Blast Mitigation System

ARO Proposal Number: 60050-EG

ARO Grant Number: W911-NF-11-1-0518

Project Period: 10/17/2011 to 01/16/2015

Mica Grujicic (PI)

Department of Mechanical Engineering, Clemson University

241 Fluor Daniel EIB, Clemson University, Clemson, SC 29634-0921

Table of Contents

1. Problem Statement and Objectives

The High Mobility Multipurpose Wheeled Vehicle (HMMWV), Figure 1(a) [1], is the prototypical light tactical vehicle which has been used by the US military for over 20 years. This vehicle was developed and deployed for conventional military conflict with well-defined frontlines, and was intended for use behind the frontline. Consequently, and not surprisingly, the HMMWV has been found lacking the necessary blast and ballistic resistance in the recent and the ongoing asymmetric warfare, in which the distinction between frontline combat and transportation convoys has been severely blurred [2, 3]. For this reason, HMMWVs have mostly been replaced, in the past conflict in Iraq and the ongoing conflict in Afghanistan, by bigger, heavier MRAP (Mine Resistant Ambush Protected) vehicles, Figure 1(b) [4], which have been specifically designed for resistance to IEDs (Improvised Explosive Devices) blast. The MRAP vehicles have their own limitations, including: (a) reduced tactical mobility/utility; (b) limited maneuverability on crowded city streets; (c) inferior fuel economy; and (d) significantly reduced deployability (these vehicles are too heavy to be driven over 70% of the world's bridges [5]) and transportability (the MRAP vehicle weight typically exceeds the payload capacity of the CH-47 Chinook helicopter).

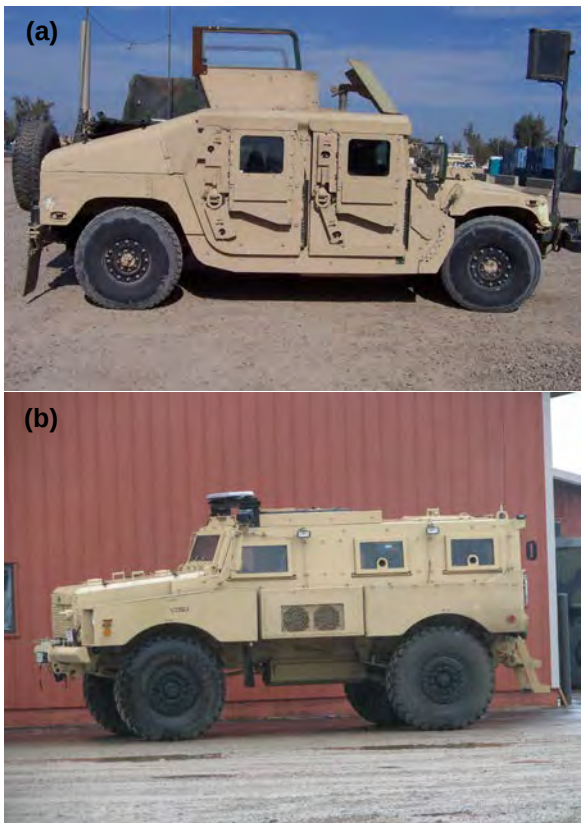

Figure 1. Typical light tactical vehicles currently used by the US military: (a) High Mobility Multipurpose Wheeled Vehicle (HMMWV) [1]; and (b) Mine Resistant Ambush Protected (MRAP) vehicle [4].

To address the limitations of light tactical vehicles mentioned above, the US military continues to seek innovative concepts and solutions which: (a) can improve blast-survivability of these vehicles; and (b) do so without compromising vehicle

mobility/maneuverability, transportability, deployability or fuel economy. One of the concepts currently being used in the light tactical vehicles is the V-shaped vehicle hull (or simply V-hull). The two most common renditions of the V-hull are depicted schematically in Figures 2(a)–(b). In the case of the standard V-hull solution, Figure 2(a), the blast-mitigation performance (as measured by the reduction in the momentum transferred to the vehicle by the gaseous detonation products, soil ejecta and mine casing) is improved as the V-hull is made steeper. However, the maximum steepness is constrained by the requirements related to the minimum acceptable vehicle ground clearance and the maximum acceptable cabin-floor height. In the case of the truncated V-hull design, Figure 2(b), V-hull steepness is increased at the expense of introducing a flat bottom portion of the V-hull. Due to the tradeoff between the benefits (i.e. decreased blast impulse) offered by the increased steepness of the V-hull and the penalty (i.e. increased blast impulse) incurred due to the small flat section, and depending on the location of the detonated mine or IED, this design may or may not result in an improved blast-mitigation performance relative to that offered by the standard V-hull design (both associated with the same vehicle ground clearance and cabin-floor height).

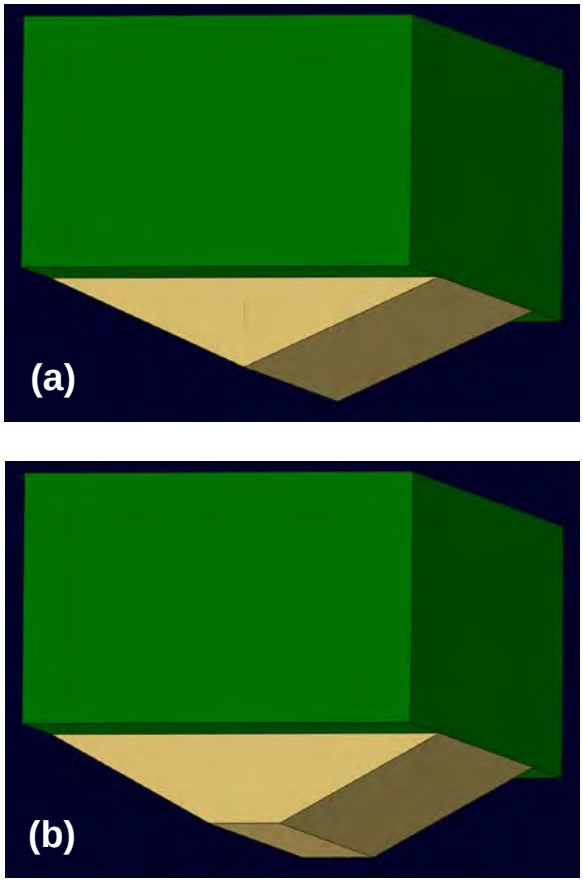

Figure 2. Two most common renditions of the V-shaped hull concept/solution: (a) standard V-shaped hull; and (b) truncated V-shaped hull.

Another concept aimed at improving the blast survivability of the tactical vehicles is the integration of the so-called blast chimney into the conventional HMMWV. The blast chimney is simply a vertical channel which connects the vehicle bottom to its roof and

enables the venting of soil ejecta, gaseous detonation products and mine casing fragments [6, 7] resulting from a mine blast underneath the vehicle. Due to the sensitive nature of the subject matter, relatively little has been reported in the open literature regarding the blast-mitigation potential of the blast chimney concept. Nevertheless, it is suggested that the blast chimney improves the blast-survivability of light tactical vehicles beyond the level offered by the V-shaped hull of the vehicle in two ways: (a) by enabling venting of soil ejecta, gaseous detonation products and mine casing fragments (and thus lowering the blast impulse transferred to the vehicle); and (b) by creating a downward thrust on the vehicle via the promotion of supersonic expansion of gaseous detonation products exiting the blast chimney [8] (and thus lowering the possibility for the vehicle lift-off from the ground). To highlight the additional blast-mitigation effect offered by the blast chimney, simple schematics of three vehicle hull configurations/geometries are depicted in Figures 3(a)–(c). The conventional V-hull is depicted in Figure 3(a). In this case, the blast mitigation performance increases with an increase in the V-hull steepness. However, constraints associated with vehicle ground clearance and height limit the maximum allowable V-hull steepness. A truncated V-hull design is depicted in Figure 3(b). In this case, the blast mitigation performance is enhanced

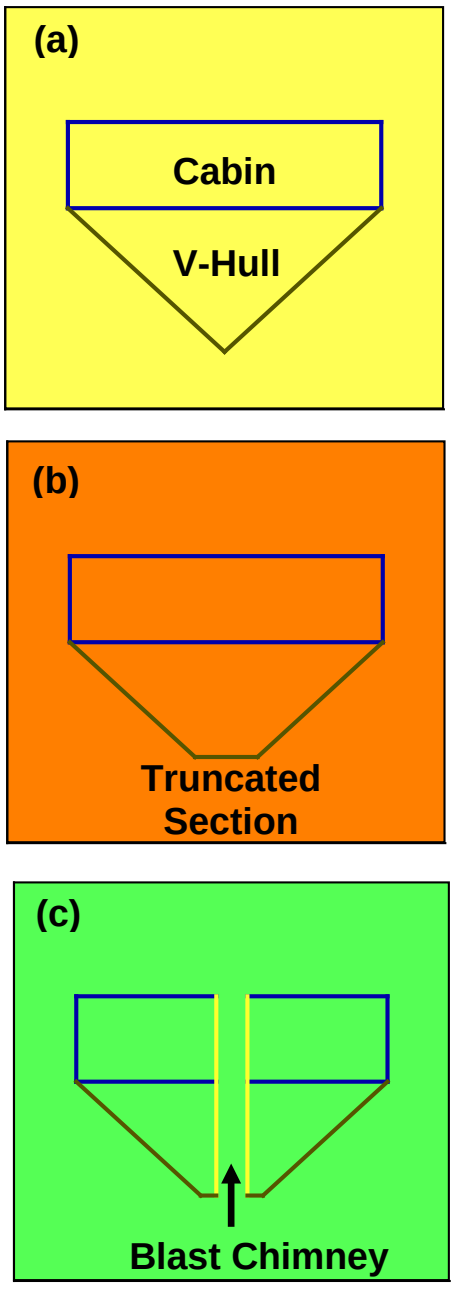

Figure 3. Three blast-mitigation vehicle-hull concepts: (a) V-shaped hull; (b) truncated V-shaped hull; and (c) same as (b) but with addition of a blast chimney.

relative to that offered by the design depicted in Figure 3(a) since the benefits (decreased blast impulse) offered by the increased steepness of the V-hull outweighs the penalty (i.e. increased blast impulse) incurred due to the small flat section. As seen in Figure 3(c), incorporation of a chimney, allows the gaseous detonation products, soil ejecta and mine-casing fragments under the chimney to be vented, while still permitting high-steepness V-hull sides [8].

While the blast-chimney concept offers benefits relative to the reduction in the blast momentum transferred to the target vehicle, it is also associated with at least two major shortcomings: (a) not surprisingly, it has been found that the incorporation of the chimney which runs through the vehicle cabin limits the mobility of the occupants within the vehicle and their ability to survey the surroundings [7]; and (b) off-road vehicle-testing performance studies have indicated a loss in the vehicle structural reliability and durability which has been currently attributed to the enhanced rate of vehicle-frame fatigue-induced failure which, in turn, has been linked with the aforementioned increased cabin rigidity [7].

The main objective of this project was to address the aforementioned limitations of the blast-chimney concept related to the loss of cabin space, ability of the vehicle occupants to scout the environment and degradation of the vehicle's structural durability/reliability. Towards that end, a new blast-mitigation concept, referred to as the "side-vent-channels concept" hereafter, has been developed and analyzed computationally [9]. As shown schematically in Figure 4, this concept utilizes side vent tubes/channels (of the appropriate cross sectional shape and wall thickness) attached to the V-shaped vehicle underbody and open at both ends. The bottom end of each tube is cut parallel to the ground (to promote inflow of the detonation by-products and soil ejecta and to prevent structural collapse, crushing, of the tube inlet under blast loads) and flush with the V-hull bottom. The channels/tubes are intended to function as exhaust nozzles as in the case of the pulse-detonation engine and, thus, provide a downward thrust to the vehicle. The secondary role of the channels/tubes is to reduce the blast momentum transferred to the targeted vehicle by enabling the venting of the gaseous detonation products, soil ejecta and mine-casing fragments. The geometry of the side-vent-channels is optimized with respect to the attainment of the maximum downward thrust on the vehicle by coupling an optimization

algorithm with a computational analysis (analogous to the one often employed in the case of design of pulse-detonation rocket engines). It should be noted that in order to prevent potential misuse, of the ideas proposed and the results obtained in the present work, the term "vehicle" has been replaced in Figure 4 as well as in the remainder of this document with the term "surrogate box structure" (SBS).

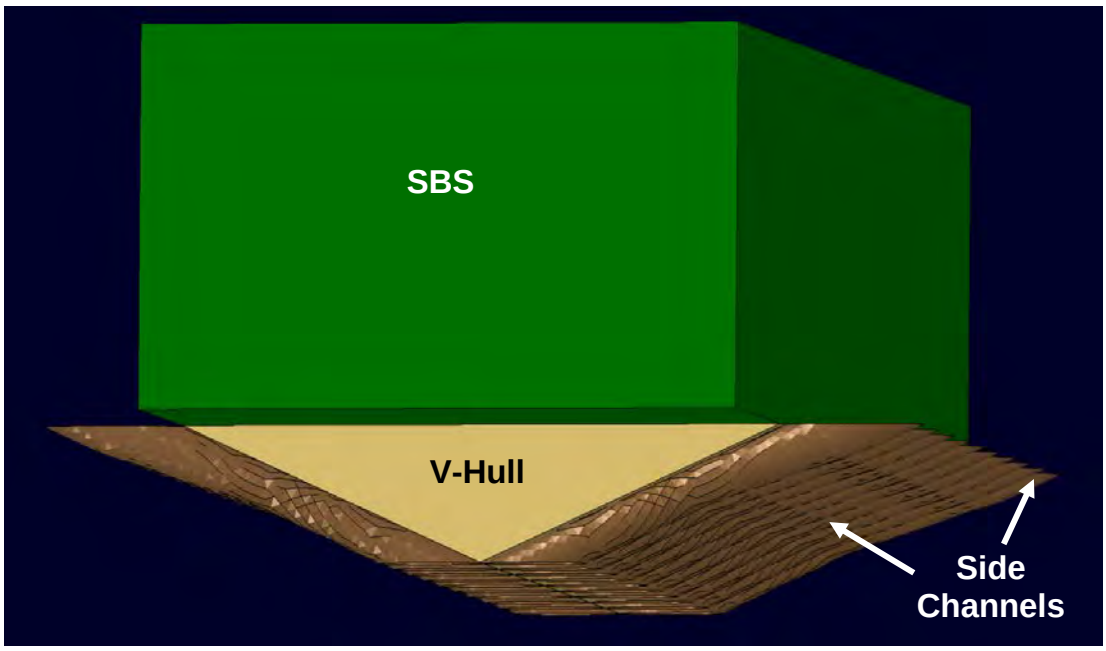

Figure 4. Side channels/tubes based blast-mitigation concept originally proposed in Ref. [9]. Note that the abbreviation SBS stands for "surrogate box structure."

2. Approach

In the present work, all computational analyses were carried out using a new combined finite-element/discrete-particle/fluid-continuum computational approach [10, 11]. In Section 2.1, details are presented regarding: (i) the formulation of the basic problem related to the detonation of a shallow-buried mine and subsequent impulse loading experienced by the target SBS through its interaction with the detonation products and soil ejecta; and (ii) the computational approach utilized in the examination of the side-vent-channel solution and its blast-mitigation capacity. Furthermore, an optimization approach was utilized to determine the optimum configuration of the side-vent-channel blast-

mitigation solution. The optimization analysis employed, the selection of the design variables, and the definition of the objective functions, are all discussed in Section 2.2.

2.1. Analysis of the Mine-blast

The basic problem analyzed in the present work involves detonation of a mine shallow-buried underneath the targeted SBS (equipped with the V-shaped hull, with or without side-vent-channels), and the subsequent interaction of gaseous detonation products, soil ejecta and blast waves with the SBS underbody. Details regarding the recasting of this physical problem into the corresponding mathematical model and the computational techniques used to investigate this problem and to establish blast-mitigation potential of the side-vent-channel solution are presented in the following subsections.

2.1.1. Computational Domain

The computational domain used consists of three distinct sub-domains, Figure 5: (a) a continuum-structure Lagrangian-type; (b) a dispersed discrete-particle Lagrangian-type; and (c) a fluid-continuum Eulerian-type.

The continuum-structure sub-domain is associated with the SBS (equipped with the V-hull, with or without side-vent-channels) and modeled using three-noded shell elements. Depending on the SBS configuration modeled, the number of finite elements ranged between ca. 60,000 and 80,000. In the majority of the computational analyses, the SBS was rigidized (in order to reduce the computational cost). In a few remaining analyses, flexibility/deformability and damage/structural-failure of the SBS was taken into account (mainly to demonstrate that the present model can successfully incorporate these important effects). Close examination of Figure 5 reveals that the geometry of the continuum-structure sub-domain has been modified relative to the one displayed in Figure 4. Specifically, in place of a constant-angle V-hull, a two-angle V-hull design is utilized. Since in the latter design, the side of the V-hull possesses two sections with differing inclinations, additional degrees of freedom are created within the V-hull design space which could be adjusted for maximum blast-mitigation performance. A more detailed discussion of this topic will be given below. Additional modifications made in the SBS geometrical model concern the use of added masses of proper magnitude and placement to account for the components such as engine,

drive-train, wheels, turret, cabin interior including the occupants, etc. This was done in order to improve the fidelity of the SBS rigid model with respect to the total mass and the overall moment of inertia.

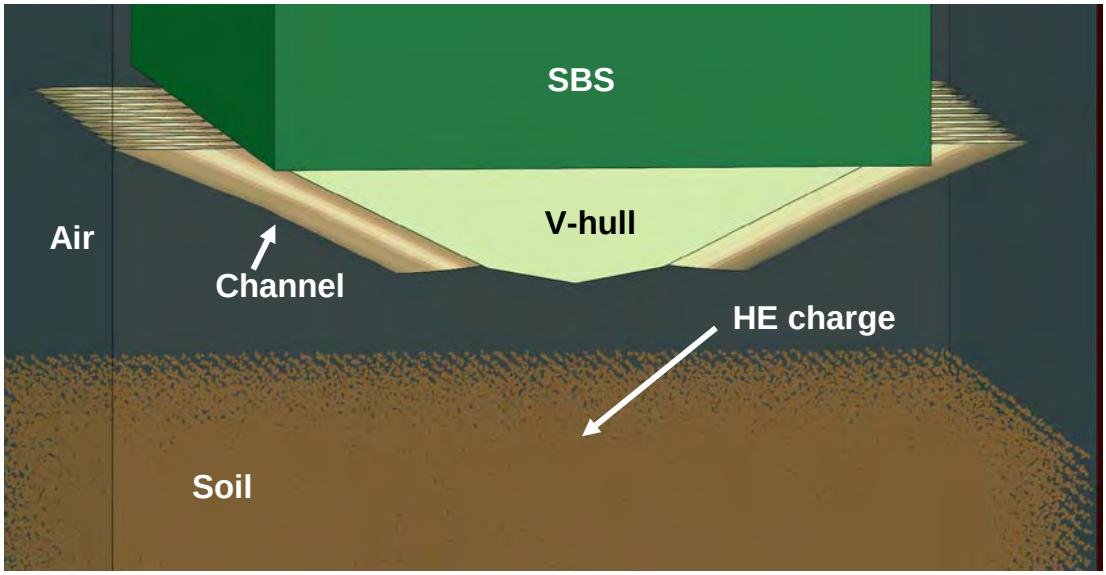

Figure 5. A prototypical computational domain used in the combined three-dimensional finite-element/discrete-particle/fluid-continuum analysis of the buried-mine detonation event and the subsequent interactions of the detonation products, soil ejecta and air-blast with the SBS equipped with a V-hull and side vent channels. Please note that the mine is shallow-buried and its view is obstructed by the surrounding soil.

As far as the discrete-particle sub-domain is concerned, it comprises soil particles (mine-casing fragments are not modeled explicitly). The discrete-particle sub-domain possesses a rectangular parallelepiped external shape and is placed at the appropriate SOD from the SBS. Except for a circular-disk-shaped region placed at the appropriate DOB, and filled with the mine (or more precisely, high-pressure gaseous detonation products), the domain is filled randomly with the soil particles to achieve the desired packing-density of the soil. Following our prior work [12], in which the effect of the number of soil particles (or, alternatively, the size of the soil super-particles), was investigated, the number of discrete particles used was ca. 140,000–160,000.

The fluid-continuum Eulerian sub-domain is of a rectangular-parallelepiped geometry and, initially, envelops the other two sub-domains. It is meshed using cubic-shape cells.

After conducting a preliminary cell-size sensitivity analysis, the number of Eulerian cells was set to ca. 600,000–800,000.

Initial configurations of the three computational sub-domains utilized in the present work are depicted in Figure 5. It should be noted that the SBS structure possesses two vertical planes of symmetry, suggesting that only one-quarter of the computational domain needs to be analyzed explicitly. However, due to the asymmetric distribution of the velocities of ejected soil particles, the entire computational domain was analyzed. By analyzing the entire computational domain, rather than one of its quarters, potential lateral translation and rotation of the SBS are also enabled.

2.1.2. Combined Finite-Element/Discrete-Particle/Fluid-Continuum Approach

As mentioned earlier, within the computational approach used in the present work: (a) the SBS is modeled as a (either deformable or non-deformable) finite-element continuum structure; (b) soil ejecta are modeled as discrete particles; while (c) the gaseous detonation products and air are modeled as a fluid continuum. To completely define the computational model of the problem under investigation, the following functional relationships must be defined: (i) governing conservation equations; (ii) functional relations controlling interactions between materials of the same (e.g. soil granules) and different (e.g. gaseous detonation products and soil particles) types; (iii) material-specific constitutive relations defining the mechanical behavior of the attendant materials under different kinematic and kinetic conditions; and (iv) other auxiliary relations such as the initial and the boundary conditions. These relationships are briefly overviewed in the remaining subsections.

Structural Finite-Element Formulation

As mentioned earlier, the SBS is modeled in the present work either as a deformable or a rigid structure. In the cases when the SBS was modeled as a deformable structure, the conventional displacement-/stiffness-based finite-element formulation was employed. Within this formulation, the subject (continuum-type) structure is first discretized into a number of finite-size interconnected elements. Next, the governing mass and momentum conservation equations for the structure are recast at the level of individual elements, combined with the associated material constitutive relations and initial/boundary/loading-conditions, integrated

out, and assembled into a system of algebraic equations. The system of equations is next solved using one of the matrix-type linear/nonlinear solution algorithms in order to determine the mechanical/dynamic response of the structure subjected to the prescribed loading and kinematic constraints. Since the basic matrix-type equations for the finite-element method described here can be found in many texts and published papers, e.g. [13], these equations will not be presented in this document.

In the cases when the SBS is treated as a rigid structure, the SBS model includes specification of the following: (a) mass; (b) location of the center of mass (COM); and (c) the moment of inertia second order tensor relative to the COM. These quantities are determined from the knowledge of the mass and COM of individual elements through the application of standard functional relations for an assembly of discrete particles (finite-elements, in the present case). Since these relations can be found in many texts and published papers (e.g. [14]), they will not be repeated here.

Discrete-Particle Formulation

Within this formulation, each attendant material (soil granules) is represented as an assembly of discrete, rigid, spherical, interacting particles which exchange momentum and kinetic energy during their collisions/contact with each other and with the finite-element-based SBS and the continuum-fluid-based gaseous detonation products and air. Typically, to make the computational cost manageable, groups of individual particles are first clumped into "*super-particles*" (referred to simply as particles hereafter) and the analysis is carried out using the latter. Due to its Lagrangian character, this formulation has a number of advantages in comparison to the Eulerian-based formulations [12].

Within this formulation, particle motion involves both translation and rotation, and is governed by the force-based and moment-based Newton's second law as:

$$m_i \frac{d\mathbf{v}_i}{dt} = \sum_k \mathbf{F}_{ik} \tag{1}$$

$$I_i \frac{d\boldsymbol{\omega}_i}{dt} = \sum_k \mathbf{M}_{ik} \tag{2}$$

where subscript i is the particle label, m is the particle mass, $\mathbf{v}$ is the particle linear velocity, t is the time, $\sum_k \mathbf{F}_{ik}$ is the interaction force, subscript k is the interaction label, I is the moment of inertia, $\boldsymbol{\omega}$ is the particle angular velocity, and $\sum_k \mathbf{M}_{ik}$ is the interaction moment. In Eqs. (1)–(2), subscript k was used to denote different types of interactions, such as particle/particle, particle/vicinal-fluid, and particle/structure interaction forces and moments. As a result of these interactions, momentum and energy are exchanged.

Fluid-Continuum Formulation

Within this formulation, the behavior of the fluid material(s) (gaseous detonation products and air) is governed by the continuity and Navier-Stokes equations. However, in order to account for the fact that a portion of the space containing the fluid materials is occupied by the discrete-particle (and, perhaps, the structural-continuum) materials, and the fact that the fluid may be a mixture of materials, the locally-averaged continuity and Navier-Stokes equations for flow through a porous medium are used as:

$$\frac{\partial \varepsilon}{\partial t} + \nabla \cdot \left(\varepsilon \mathbf{u}_f \right) = 0 \tag{3}$$

$$\frac{\partial \left(\rho_f \varepsilon \mathbf{u}_f \right)}{\partial t} + \nabla \cdot \left(\rho_f \varepsilon \mathbf{u}_f \mathbf{u}_f \right) = -\nabla p - \mathbf{F} + \nabla \cdot \left(\varepsilon \tau \right) + \rho_f \varepsilon \mathbf{g} \tag{4}$$

where the subscript f is used to denote a fluid-based quantity, ε is the local porosity, $\mathbf{u}_f$ is the fluid velocity, ρ_f is the fluid density, p is the pressure, $\mathbf{F}$ is the volumetric particle-fluid interaction force, τ is the fluid viscous stress tensor, and $\mathbf{g}$ is the gravitational acceleration.

Interactions

In general, within the computational analyses such as the one carried out in the present work, provisions must be made for interactions between the same, same type, and different types of materials. The number of interaction types is greatly reduced in the present case due to the fact that there is one structural continuum material (SBS), one discrete-particle material (soil), and a two-material fluid mixture (consisting of gaseous detonation products and air). In fact, neglecting some of the secondary details related to the nature of the

contacting materials, only two basic types of interactions are identified in the present work: (a) particle/particle and particle/SBS interactions; and (b) fluid/particle and fluid/SBS interactions. These two types of interactions are briefly overviewed below.

Particle/Particle and Particle/SBS Interactions: While the description presented below pertains explicitly to the case of particle/particle interactions, it is equally applicable to the particle/SBS interactions. Particle/particle interactions are modeled in the present work using the so-called penalty contact algorithm [15] rather than the computationally-efficient (but physically over-simplified) elastic (or, more precisely, kinematic-elastic) collision algorithm. This was done in order to account for the effects such as: (i) soil-particle finite stiffness; (ii) rate-dependent dissipative/damping nature of the inter-particle collisions; and (iii) the inter-particle frictional effects.

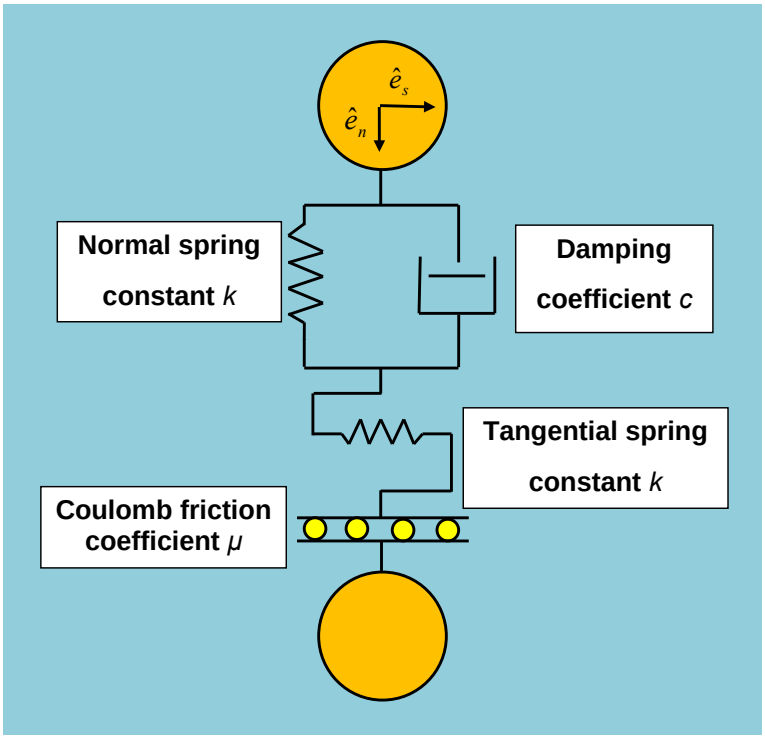

Figure 6. A schematic of the contact-mechanics model involving two interacting equal-sized/mass spherical particles of soil.

The essential features of the two-particle penalty-contact model used are depicted schematically in Figure 6. Within this model, particle normal interactions are accounted for by a linear spring (with a spring constant k) and a linear dashpot (with a damping coefficient c) connected in parallel. As far as the tangential interactions are concerned, they are modeled using a linear spring (also of stiffness k) and a Coulomb frictional element (which is characterized by a friction coefficient μ and which limits the tangential-spring force). The

values of the four interaction parameters (k, c, μ and ξ) for the cases of dry and saturated soil particle/particle interactions (as well as for the corresponding particle/SBS interactions) were determined in our recent work [12].

Fluid/Particle and Fluid/SBS Interactions: Determination and quantification of the interactions between the Eulerian fluids and Lagrangian solids is often quite a challenging problem, due to the fact that the associated sub-domains generally do not possess conformal meshes. This problem is compounded in cases in which the size of discrete particles is relatively small in comparison to the Eulerian-mesh cell size. In such cases, various approximation/simplification schemes such as the so-called "two fluid model" [16] and "computational fluid dynamics – discrete element method (CFD-DEM)" [17] are used. Within these schemes, different approximations/simplifications are utilized in order to account for the presence of the discrete particles within the fluid, without explicitly representing/modeling these particles. Fortunately, in the present case, the size of the discrete particles (i.e. soil granules) is comparable to that of the Eulerian-mesh cell, and these over-simplified algorithms do not have to be used. Instead, the so-called "immersed boundary method" [18] is employed in the present work in order to model fluid/particle and fluid/SBS interactions. This method is specially designed for non-conformal meshes and, hence, its first task is to identify, during each computational time increment, the boundary between the Eulerian sub-domain region and the Lagrangian (discrete-particle or SBS) sub-domain. Subsequently, the method enforces Eulerian-Lagrangian contact constraints using the aforementioned penalty method, within which the extent of contact pressure is governed by the local surface penetrations (where the default penalty stiffness parameter is automatically maximized subject to stability limits). As far as the shear stresses are concerned, they are transferred via a "*slip/stick*" algorithm, that is, shear stresses lower than the frictional shear stress are transferred without interface sliding (otherwise interface sliding takes place). The frictional shear stress is defined by a modified Coulomb law within which there is an upper limit to this quantity. In the case of rigid-discrete particles and rigid SBS, this quantity is set to infinity while in the case of the deformable SBS, it is set to the shear strength of the SBS material. The frictional shear stress is then defined as the smaller of the product between the

static/kinetic friction coefficient and the contact pressure, on the one hand, and the Lagrangian-material shear strength, on the other.

Material Models

Since the present model consists of three computational sub-domains, separate constitutive models are defined, in the remainder of this section, for all the materials residing within the sub-domains.

Lagrangian SBS Sub-domain: In the cases when the SBS was modeled as a rigid structure (i.e. in the majority of the cases analyzed), the only material parameter which had to be defined was the mass density (set to 7850 kg/m^3, a typical value for steel). On the other hand, when the SBS was modeled as a deformable structure, it was assumed to be made of a conventional AISI 4340 steel whose deformation and failure constitutive response could be represented using the Johnson-Cook material model [19]. Since a detailed overview of this material model including its AISI 4340 parameterization can be found in our recent work [19, 20], similar details will not be presented here.

Lagrangian Discrete-Particle Sub-domain: Within the present formulation, soil particles are explicitly considered as being rigid (i.e. non-deformable). However, the effective stiffness of the soil particles is not infinite but rather of a finite value. The reason for this is that, as discussed above, particle/particle and particle/SBS interactions are assumed to be of a non-rigid elastic type, but rather to be associated with finite values of the normal and shear contact-spring stiffnesses. In other words, the (non-rigid) constitutive response of the soil particles is recovered through the use of the non-rigid penalty-contact algorithm.

Eulerian-fluid Sub-domain: This sub-domain contains a mixture of two fluids, i.e. air and gaseous detonation products. For fluids, the material constitutive behavior is described by: (a) an equation of state, EOS (a functional relationship between pressure, mass-density/specific-volume and internal-energy-density/temperature); and (b) a functional relationship between the shear stress and the shear strain and strain-rate. Two types of EOS were utilized in the present work: (i) ideal gas EOS; and (ii) Jones-Wilkins-Lee (JWL) EOS [21]. These two types of EOS are typically selected in the analysis of various

detonation/explosion scenarios. Since a detailed overview of the ideal-gas and JWL EOS relationships for the air/detonation-products mixture and their parameterization for the case of C-4 high explosive (HE), the explosive utilized in the present work, can be found in our prior work [22–24], the same details will not be repeated here.

Since the air/detonation-products mixture is gaseous, it has a zero effective shear stiffness. Thus, shear strain within this material does not generate shear stress. However, shear stresses can be developed as a result of a gradient in the flow velocity, i.e. shear-strain-rate. In the present work, the Newtonian-fluid model is adopted for the gaseous mixture, within which the shear stress is assumed to scale linearly with the velocity gradient (with the proportionality constant, the viscosity, being set at $1.78 \cdot 10^{-5}$ Pa·s.).

It should be noted that, within the current formulation, the initially unexploded mine made of C-4, a solid material, is not modeled explicitly. Rather, detonation is treated as an instantaneous process which converts, at the beginning of the computational analysis, unreacted explosive into high-pressure, high-temperature gaseous detonation products. This is the reason why no material model had to be defined for the (solid) C-4 HE.

Computational-Analysis Type

The mine blast event and the subsequent interactions between the detonation products, soil ejecta and air blasts with the SBS are analyzed computationally using the combined finite-element/discrete-particle/fluid-continuum algorithm. Due to the extremely short duration of the mine-blast detonation event (ca. tens of milliseconds), heat transfer between the Eulerian and Lagrangian sub-domains, as well as heat transfer by conduction within the fluid sub-domain, are not considered. In other words, only convective heat transfer within the fluid is considered.

Initial Conditions

Prior to the beginning of the computational analysis, the Eulerian sub-domain is filled with atmospheric-pressure/room-temperature air except for the “mine region,” which is filled with high-pressure, high-temperature gaseous detonation products. Then the soil-discrete-particle sub-domain is placed in the lower portion of the Eulerian sub-domain. Filling of the former sub-domain with soil particles, to achieve the desired packing density, is carried out

in accordance with the procedure described in our prior work [12]. This procedure ensures that no "inter-particle penetration" (except the one caused by gravity) exists between the neighboring soil particles. The particles are assumed to initially be at rest. Lastly, the continuum-Lagrangian SBS sub-domain is placed in the upper portion of the Eulerian sub-domain at the desired SOD. The SBS sub-domain is assumed to initially be stationary and, in the case of the non-rigid SBS, to be stress-free.

Boundary Conditions

The Eulerian sub-domain is subjected, over its external faces, to the no-inflow and (101.3 kPa external pressure) free-outflow boundary conditions. The discrete-particle sub-domain is subjected, over its bottom and lateral four faces, to the non-reflecting outflow boundary conditions (in order to avoid unphysical reflection of the shock waves from these boundaries). On the other hand, no displacement/stress boundary conditions are applied over the top face of the discrete-particle sub-domain. Except for loading due to gravity, no boundary conditions are applied to the SBS sub-domain.

Computational Algorithm

The computational model described in the preceding sections is analyzed numerically using the so-called CEL (Combined Eulerian-Lagrangian) algorithm, as implemented in ABAQUS/Explicit [25], a general-purpose finite-element solver. This algorithm enables an analysis of the interactions between Eulerian and Lagrangian sub-domains. Within the continuum-type Lagrangian sub-domains (SBS, in the present case): (a) the mesh (nodes and elements) is attached to the associated material and moves and deforms with it; and (b) each element must be fully filled with a single material. On the other hand, within an Eulerian sub-domain: (a) the mesh is fixed in space and the material flows through it; (b) elements/cells are allowed to be partially filled and/or contain multiple materials; and (c) since the material and the element boundaries do not generally coincide, a separate ("interface reconstruction") algorithm must be used to track the position of Eulerian material boundaries. The interface reconstruction algorithm approximates the material boundaries within an element as simple planar facets and, hence, accurate determination of a material's location within an element requires the use of fine Eulerian meshes. Since, within the present

formulation, the two Eulerian materials (air and gaseous detonation products) are assumed to be mixed at the molecular level, Eulerian-material boundaries did not need to be tracked, and relatively larger Eulerian cells could be used (making the computational analysis more efficient).

Typically, the following sequence of computational steps is carried out within each time increment: (a) Eulerian/Lagrangian interaction algorithm is used to determine loading experienced by the Lagrangian sub-domain(s); (b) conventional displacement-based finite-element analysis is carried out to update the deformation state and the position of the Lagrangian domains; (c) the current position of the Lagrangian domains is used to redefine the fluid-filled Eulerian sub-domain; (d) governing equations for the fluid are then solved as a two-step process: (i) within the so-called Lagrangian sub-step, the Eulerian sub-domain is temporarily treated as being of a Lagrangian character (i.e. its nodes and elements are attached to and forced to move with the underlying material); and (ii) within the so-called "remap" step, the distorted Eulerian mesh is mapped onto the original Eulerian mesh and the accompanying material transport is computed and used to update the Eulerian-material states and inter-material boundaries (when required).

Computational Accuracy, Stability and Cost

A standard particle-size and mesh-refinement sensitivity analysis was carried out in order to ensure that a convergence of the key results is reached with respect to the further refinement of these geometrical/mesh parameters. Due to the conditionally-stable nature of the explicit finite element analysis used, the maximum time increment during each computational step had to be kept lower than the attendant stable time increment. A typical 50 ms computational analysis followed by a detailed post-processing data reduction procedure required on average 2 hours of (wall-clock) time on a 12-core, 3.0 GHz machine with 16 GB of memory.

2.2. Shape/Size Optimization of V-Hull/Side-Vent-Channel

In this section, first a brief description is given of the procedure (known as the simplex algorithm) used to optimize the V-hull and side-vent-channel geometrical parameters. Then a list of these geometrical parameters (and their constraints) used in the

optimization procedure (i.e. the design variables) and the goal of optimization (i.e. the objective function) are presented.

2.2.1 Simplex Optimization Method

Geometrical optimization of the side-vent-channels is done using the basic simplex search method [26]. While the optimization problem under consideration will involve six design variables and a compound objective function, the basic idea behind the simplex method is explained here using the optimization case involving two design variables and a single objective function. The simplex optimization algorithm is associated with the following requirements/simplifications and steps:

(a) It is required that, at each step during the optimization procedure, the number of evaluations of the objective function (referred to as designs in the remainder of this paragraph) be one greater than the number of design variables. For the two-design-variable/single-objective-function optimization case, the simplex method thus requires that the objective function be initially evaluated for three (randomly-selected) pairs of design variables. In the two-dimensional search space, Figure 7, the three initial pairs of design variables form a triangle (A–B–C), which is generally referred to as the initial simplex;

(b) The three initial designs are ranked according to the values of the objective function and the type (maximization or minimization) of the optimization procedure. In the case when the objective of the optimization procedure is to maximize the objective function, the design with the smallest value of the objective function (design A in Figure 7) is ranked as worst. It should be noted that the (overall) optimum design (i.e. the design associated with a maximum value of the objective function) corresponds to a 100% point in Figure 7;

(c) Next, design A is reflected through the centroid of the other two designs to obtain a new design, design D in Figure 7. The new design replaces the prior worst design and a new simplex B–C–D is formed; and

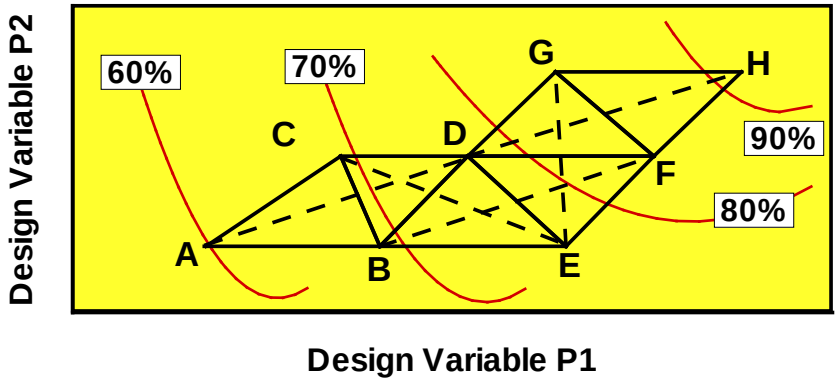

Figure 7. A schematic of the basic Simplex algorithm used for optimization of the blank shape. The initial Simplex is represented by the triangle ABC. Dashed lines with the arrow indicate replacement of the prior worst design with a new design by projection through the centroid of the remaining two prior designs.

(d) Designs within the new simplex are ranked again, the worst design, design C, identified, and the aforementioned procedure repeated. To prevent the method from bouncing back and forth between two designs in cases when the new design is the worst design within the new simplex, the simplex algorithm selects the second worst design and reflects it in such cases.

The simplex method offers the following main advantages over the alternative optimization methods [27]: (a) it does not require evaluation (a potentially costly step and sometimes infeasible step, as in the case of discrete design variables) of the derivatives of the objective function; (b) the method is quite efficient since it requires, after the initial simplex is formed, only one evaluation of the objective function per search step; and (c) in addition, the algorithm is very simple to implement and to link with a commercial finite element program such as ABAQUS/Explicit. The main limitations of the simplex method are as follows: (i) like many other optimization algorithms, it may find the local (but not necessarily the global) optimum within the design space. This limitation is typically overcome by repeating the simplex method with several different initial simplexes and selecting the best optimum; (ii) the method may require rescaling of the design variables to make them all of the same order of magnitude, since all variables are subjected to the same reflection distance; and (iii) the search progress can be slow. This limitation has been

addressed by Nelder and Mead [28] who introduced several modifications which enable expansion or contraction of the Simplex in a direction in which the optimization conditions are favorable. These modifications are, however, practical only when the number of design variables is large and when evaluation of the objective function is not expensive computationally. Since the SBS-geometry optimization problem analyzed in the present work involves a relatively small number of the design variables and the evaluation of the objective function involves a finite element simulation by ABAQUS/Explicit and post-processing of the results, which are quite time-consuming, the basic simplex search method is used.

2.2.2 Design Variables, Constraints and the Objective Function

All the SBS configurations analyzed in the present work were associated with the following geometrical dimensions: (a) box-shaped extended cabin – $L \times W \times H$ = 4.85 m × 2.2 m × 1.4 m; and (b) pentagonal-prism-shaped V-hull – $L \times W_{max} \times H$ = 3.0 m × 2.2 m × 0.5 m. To completely define the geometry of the modified V-hull, two additional parameters (design variables) need to be specified, e.g. the inclination (DV_1) and the length (DV_2) of the lower portion of the V-hull sides. The lower portion of the side-vent-channels is assumed to be of a circular cross-section and, hence, within the rigid-body framework, the cross-section is defined by only one parameter, e.g. tube radius. The upper portion of the side-vent-channels is assumed to be flared in such a way that: (i) each cross-section of the channel parallel with the ground is of an elliptical shape; and (ii) the minor axis (the one parallel with the side of the V-hull) remains constant and equal to the diameter of the lower portion of the side-vent-channel. The side-vent-channels are attached to the portion of the V-hull side associated with the higher inclination. Consequently, the attached length of the side-vent-channel is not an independent variable, but is rather defined by the modified V-hull geometrical and size parameters. The top portion of the side-vent-channels is cut flush with the ground while the bottom portion of the side-vent-channels is cut at different angles (under the constraint that the lowest point of the side-vent-channels is not lower than the V-hull bottom edge). Taking all this into account, there are four parameters characterizing the geometry and size of the side-vent-channels:

(a) circular-channel radius, DV_3. It should be noted that, since the number of channels per V-hull side is fixed at 10, the maximum radius of the channels is constrained by the condition that the adjacent channels can be in contact, but not intersect;

(b) ellipticity of the vent-channel exit cross-section, DV_4. The maximum allowable ellipticity, for a given value of the circular-section radius, is constrained by the requirement that the increase in the SBS width (due to introduction of the side-vent-channels and their flaring) does not exceed an upper bound;

(c) fraction of the attached-length of the channel over which (linear) flaring takes place, DV_5; and

(d) the angle at which the lower portion of the side-vent-channel is cut relative to the ground, DV_6.

The six design variables are depicted in Figure 8.

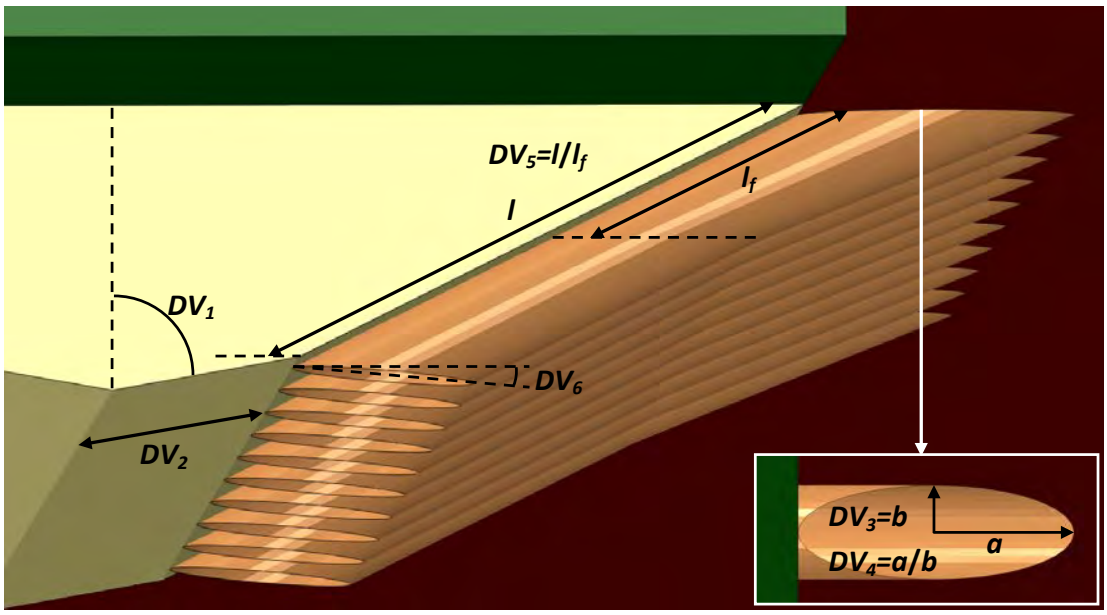

Figure 8. Definition of the six design variables, DV_1–DV_6, used in the present size and shape optimization of the SBS V-hull and the side-vent-channels.

As far as the objective function is concerned, it was defined as a weighted average of the (percent) reductions in the detonation-induced momentum transferred to, and the maximum acceleration acquired by, the SBS. In other words, the two-objective problem was recast as a single(compound)-objective problem. This approach generally does not ensure

that the best possible trade-off between the two conflicting objective functions is attained at a given level of either of the objective functions. To overcome this shortcoming of the aforementioned method based on the objective-function weighing, a true multi-objective (or, more precisely, a bi-objective) optimization approach was utilized in the present work. Within this approach, the objective function is treated as a two-component vector (rather than as a scalar). The two (conflicting) components are: (i) the reduction in the detonation-induced momentum transferred to the SBS; and (ii) the reduction in the maximum acceleration acquired by the SBS. The conflicting nature of the two objective-function components can be understood by considering the effect of the SBS mass on the two. Specifically, as the SBS mass is increased, the momentum transferred to the SBS is also increased while the maximum acceleration acquired by the SBS is decreased. Due to the conflicting character of the two objective-function components, one cannot expect a unique solution to the optimization problem. Instead, the result of the multi-objective optimization is a series of so-called "non-inferior" solutions forming the so-called "Pareto front." The unique feature of the Pareto-front optimization solutions is that there are no infinitesimally small perturbations in the design variables associated with these solutions which could simultaneously improve two or more components of the objective-function vector. In other words, such perturbations are associated with a trade-off between the objective-function vector components. To clarify this point, a schematic is shown in Figure 9 of the two-component objective-function space. The feasible portion of this space is colored yellow. In this figure, the Pareto front is represented

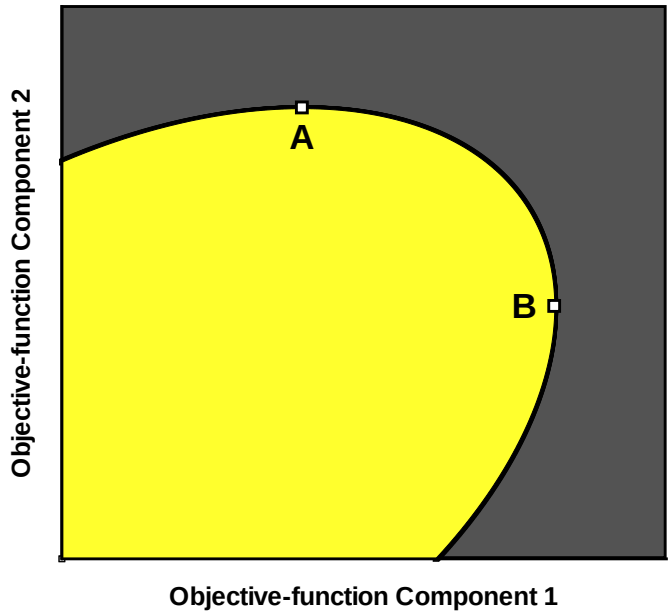

Figure 9. A schematic of the two-component objective-function space. The feasible portion of this space is colored yellow. The Pareto front is defined by curve *AB*, where *A* and *B* correspond respectively to the maximum (optimal) values of the two objective-function components.

by curve A–B, where points A and B correspond respectively to the maximum (optimal) values of the two objective-function components. In the interior portion of the objective-function feasibility space, one can always perturb the given design (as defined by the values of the two objective-function components) in order to simultaneously increase both objective-function components. No such perturbations are possible along the A–B line (since they would place the design outside the feasible domain). For this reason, the designs associated with the Pareto front A–B are generally referred to as being "non-inferior."

3. Relevance to the Army

As discussed in Section 1, light tactical military vehicles currently in use suffer from a number of deficiencies. To address these deficiencies, the US military continues to seek innovative concepts and solutions which: (a) can improve blast-survivability of these vehicles; and (b) do so without compromising vehicle mobility/maneuverability, transportability, deployability or fuel economy. The concept named "side-vent-channels" proposed and investigated computationally in the present work is aimed at addressing mine-blast survivability deficiencies of the lighter tactical vehicles like the HMMWV. To assess the blast-mitigation potential of the new concept, computational investigations are carried out which yielded the extent of momentum, kinetic energy and acceleration reductions within the targeted SBS brought about by the introduction of the side-vent-channels.

4. Accomplishments

In this section, the key accomplishments achieved in the present work are presented and discussed. First, some prototypical results yielded by the employed three-dimensional combined finite-element/discrete-particle/fluid-continuum computational model and analysis are overviewed and examined. When discussing these results, particular attention is paid to providing insight into the ability of the modified V-shaped hull and the side-vent-channels to lower the blast momentum transferred to, and the maximum associated acceleration acquired by, the SBS through the operation of venting and downward-thrust effects. In the second portion of this section, the results of the simplex-algorithm-based multi-objective optimization analysis are presented and critically assessed.

4.1 Prototypical Results

The employed computational analysis yielded the results pertaining to the temporal evolution and spatial distribution of various particle-state and continuum-field quantities such as particles' position, (translational and rotational) particle velocities, particle/particle and particle/continuum-structure interaction forces and moments, etc. In addition, results pertaining to the explosive-charge detonation-induced loading experienced by, and the subsequent response of, the SBS structure were obtained. In the remainder of this section, a few prototypical results are presented and discussed.

4.1.1. Temporal Evolution of the Attendant-Material Spatial Distribution

Spatial distribution of the non-air attendant materials (i.e., steel used in SBS construction, HE detonation products and soil) at four (1 ms, 1.5 ms, 2.5 ms, and 3.9 ms) post-detonation times in the case of a prototypical SBS equipped with a modified V-shaped hull and flared side-vent-channels is shown in Figures 10(a)–(d). In these and subsequent figures, the displayed size of the soil spherical particles was adjusted for improved clarity, and the (initial) particle positions are regularized. Furthermore, the location of the HE detonation products was displayed using the spatial distribution of the corresponding material volume fraction. Examination of the results displayed in Figures 10(a)–(d), as well as their comparison with the corresponding results (not shown for brevity) for the SBS configuration with the standard V-hull but no side-vent-channels, established that the presence of the modified V-hull with side-vent-channels helps guide the flow of the gaseous detonation products and soil-ejecta (as well as air) along the direction parallel with the side of the V-hull. Closer examination of the distribution of the soil and the detonation products within the side-vent-channels reveals that the channels closest to the mine play the dominant role in the blast-venting process. Furthermore, it is seen that the ejected soil initially retains its cohesion and relatively high density, Figure 10(a), while at later post-detonation times, ejected soil breaks up into non-bonded particles and acquires a low density, Figures 10(c)–(d).

4.1.2. Temporal Evolution of the Attendant-Material Velocities

Spatial distribution of the soil-particle, Eulerian-fluid and SBS velocities at four (1 ms, 1.5 ms, 2.5 ms, and 3.9 ms) post-detonation times for the same SBS configuration as the one referred to in conjunction with Figures 10(a)–(d), is shown in Figures 11(a)–(d). In Figures 11(a)–(d), colored arrows are used to denote the velocity magnitude and its direction for the gaseous detonation products. Only colors are used to denote the magnitude of the SBS and soil-particle velocities.

Examination of the results displayed in Figures 11(a)–(d) clearly reveals: (a) the arrival of the ejected soil-particles at the channel inlet, Figure 11(a); (b) the onset of formation of a crater within the soil, Figure 11(b); (c) a high (supersonic) exit-velocity of the gaseous detonation products leaving the channels, Figure 11(c). This finding is a potential indication of the adiabatic-expansion effects which are expected to yield a downward thrust onto the SBS; and (d) soil-particles exiting the channels with a relatively high velocity, Figure 11(d). This finding could be attributed to the combined role of the side-vent-channels in guiding the soil-particle outflow and promoting additional downward-thrust effects on the SBS (which are the result of soil-particle collisions with the interior surface of the channel away from the V-hull), along with an increase in the particle (upward) velocities.

4.1.3. SBS Velocity and Acceleration Temporal Evolution

The results presented in the previous section suggested that modification in the V-hull shape and the presence of flared side-vent channels may have a positive role in reducing the effect of buried-landmine detonation on the momentum transferred to, and the acceleration acquired by, the SBS. In this section, more quantitative results pertaining to the temporal evolution of the SBS velocity and acceleration are presented and discussed. Examples of the typical SBS (z-component-dominated, total translational) velocity vs. time and the corresponding SBS acceleration vs. time results obtained in the present work are shown in Figures 12(a)–(b), respectively. In both cases, the quantity plotted along the y-axis is normalized by its maximum value while the time is normalized by its value corresponding to the SBS maximum velocity. Examination of the results displayed in these figures shows that

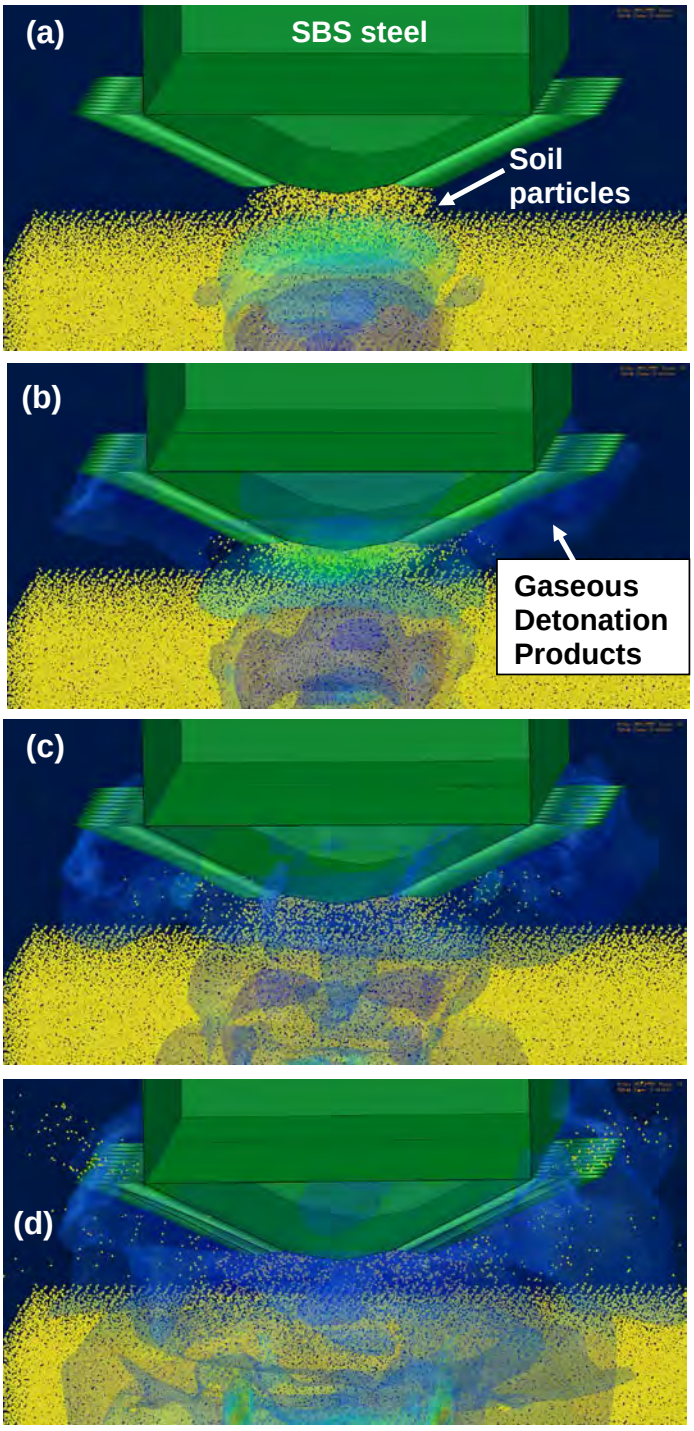

Figure 10. Spatial distribution of the non-air attendant materials (i.e., steel used in SBS construction, HE detonation products and soil), in the case of a prototypical SBS equipped with a modified V-shaped hull and flared side-vent-channels, at post-detonation times of: (a) 1 ms; (b) 1.5 ms; (c) 2.5 ms; and (d) 3.9 ms.

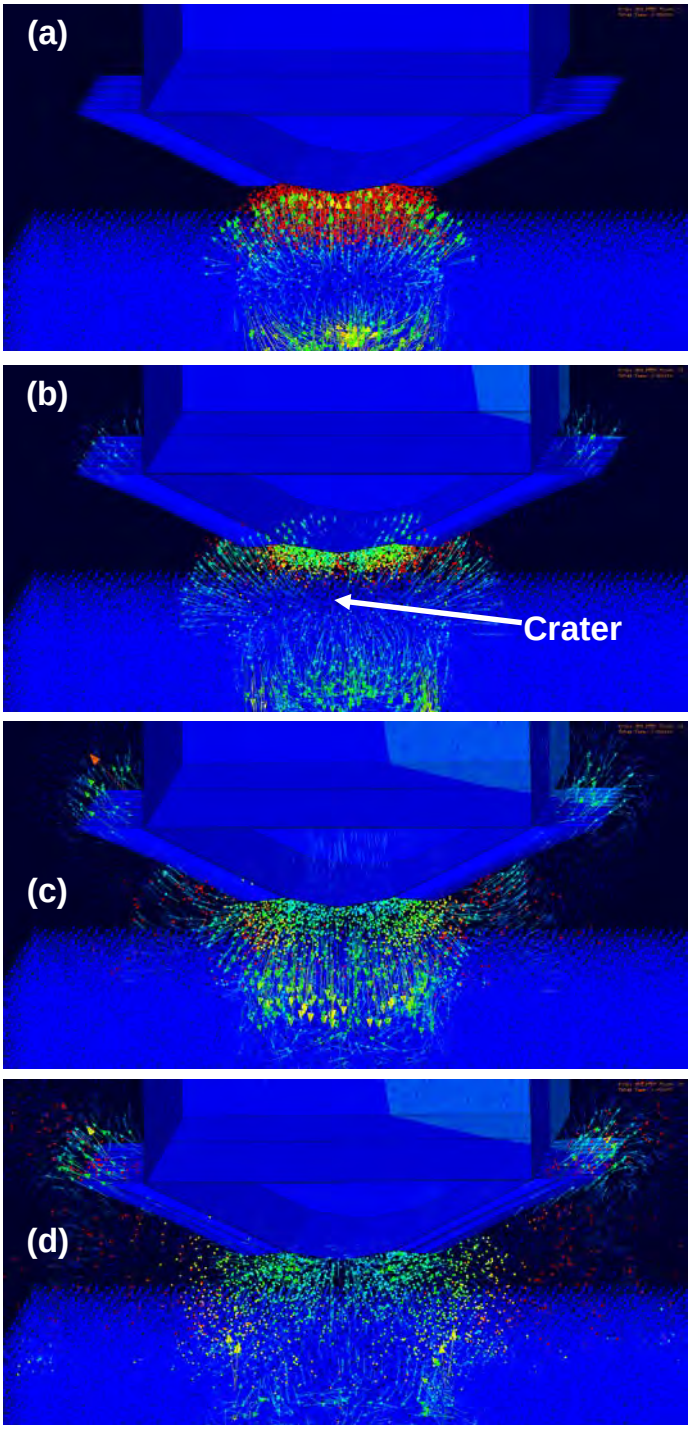

Figure 11. Spatial distribution of the soil-particle, Eulerian-fluid and SBS velocities, for the same SBS configuration as the one referred to in conjunction with Figures 10(a)–(d), at four post-detonation times of (a) 1 ms; (b) 1.5 ms; (c) 2.5 ms; and (d) 3.9 ms.

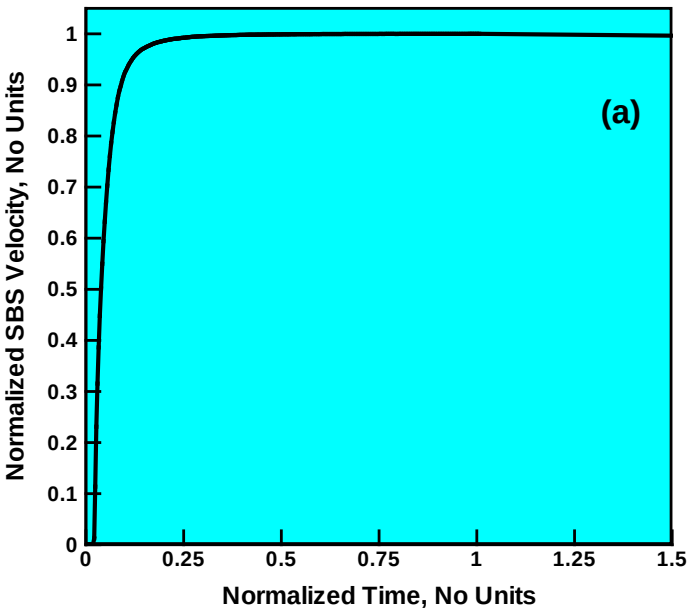

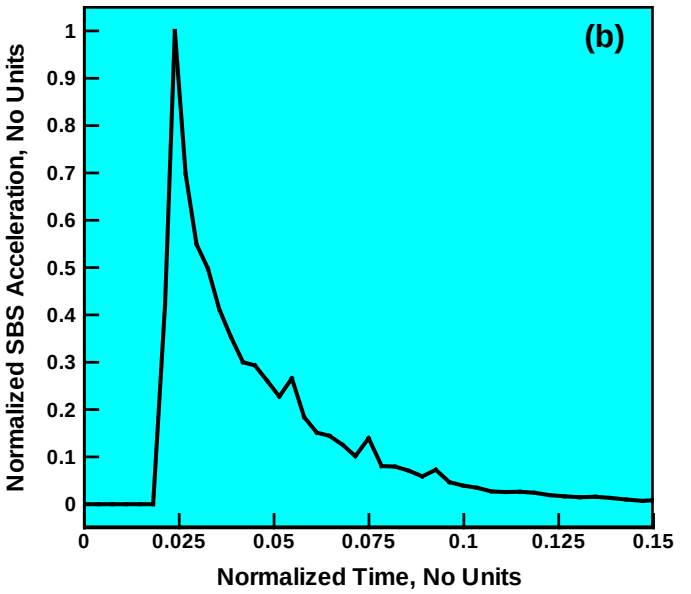

Figure 12. Examples of the typical: (a) SBS normalized-velocity vs. time; and (b) SBS normalized-acceleration vs. time results obtained in the present work.

the SBS velocity initially experiences a sharp rise, reaches a peak value and then gradually decreases under the influence of gravity. As far as acceleration is concerned, it reaches its peak value much earlier than the velocity and then sharply drops as the additional momentum transfer to the SBS from the detonation products and soil ejecta decreases.

4.2 V-Hull/Side-Vent-Channel Shape/Size Optimization

The results of the simplex-algorithm-based V-hull/side-vent-channel shape/size multi-objective optimization procedure are displayed in Figures 13, 14(a)–(f) and 15. In each of these figures, the *x*-axis represents the first component of the objective function, i.e. the percent reduction in the transferred-momentum (relative to their counterparts in the case of the SBS fitted with a standard V-hull but no side-vent-channels) residing on the Pareto front.

4.2.1. Trade-off between Objective-function Components along the Pareto Front

Variation of the second component of the objective function, i.e. the acceleration percent reduction (relative to the case of the SBS fitted with a standard V-hull but no side-vent-channels) along the Pareto front is depicted in Figure 13. Examination of the results depicted in this figure reveals that, as expected, there is a trade-off between the two components of the objective function along the Pareto front. It should be recalled that the endpoints (*A*, *B*) of the Pareto front correspond to the two single-objective optimal designs (each associated with a maximum value in the corresponding component of the multi-objective function).

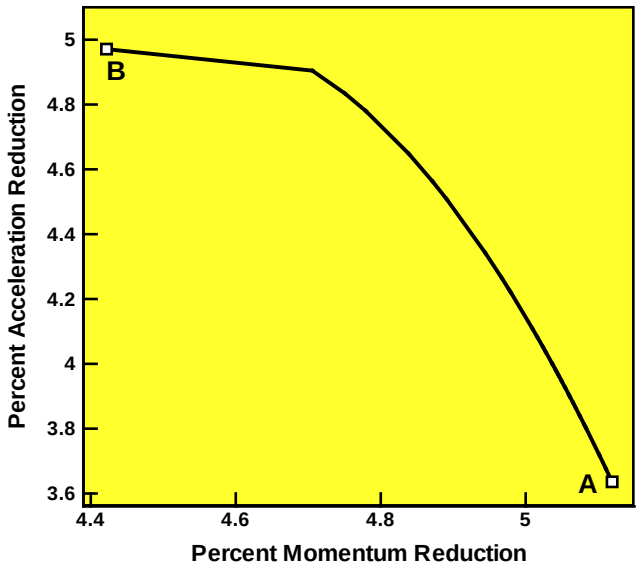

Figure 13. Variations of the two components of the objective function along the Pareto front. Please see text for definition of points *A* and *B*.

4.2.2. Optimal V-hull/Side-vent-channel Designs along the Pareto Front

Variation of the six design variables along the Pareto front is depicted in Figures 14(a)–(f). Examination of the results displayed in these figures reveals that: (a) modification of the V-hull shape from its standard configuration (as represented by the half-angle of approximately 67°) is preferred since the optimal values of DV_1 are approximately in the70–73° range, while the optimal values of DV_2 are approximately in the 0.20–0.24 m range;

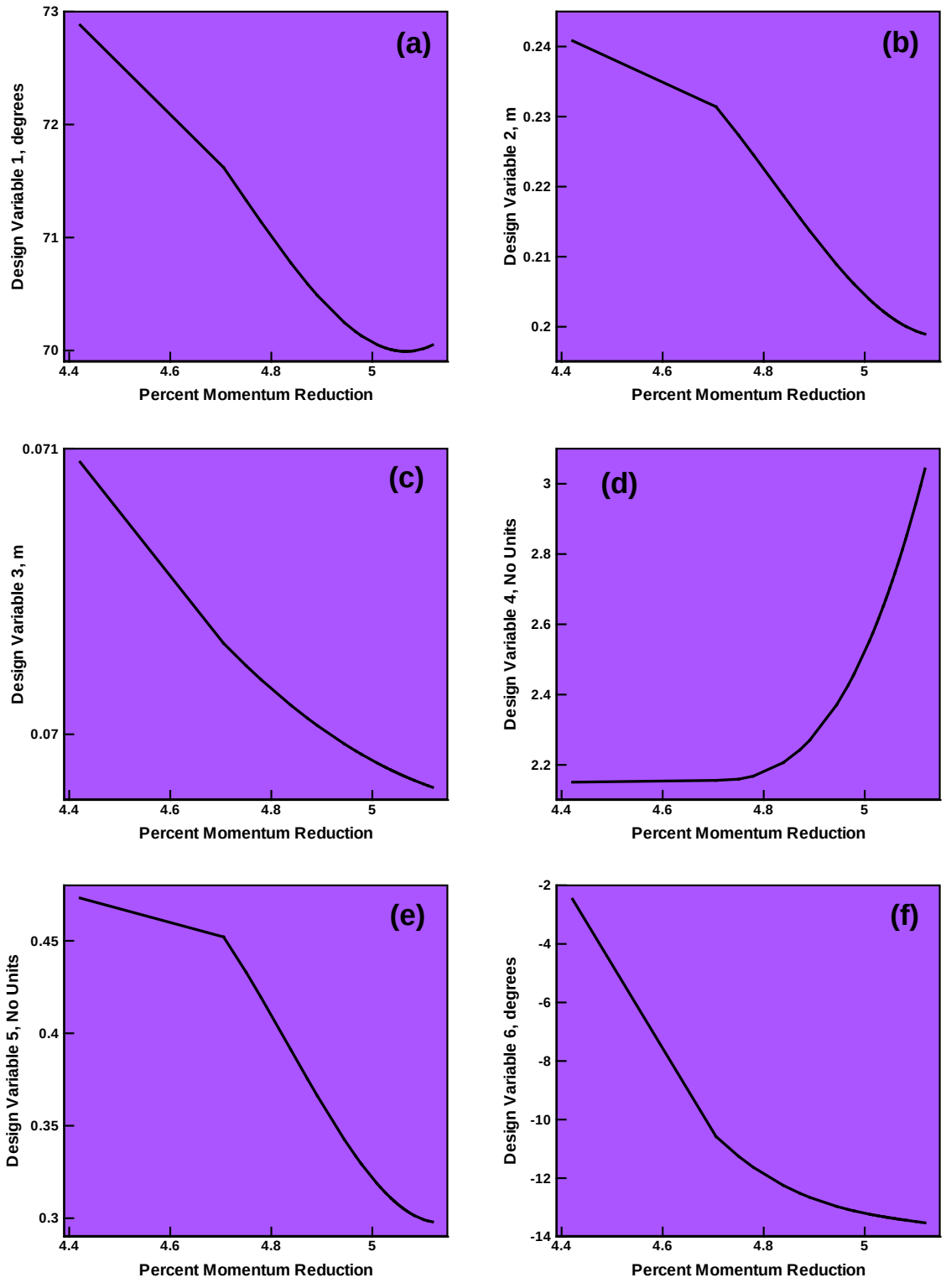

Figure 14. Variations of the six design variables along the Pareto front. Please see text for explanation of the design variables.

(b) the optimal values of DV_3 (approximately in the range 0.069–0.071 m) are very close to the maximum value of this parameter (0.071 m) corresponding to the condition of contact of the neighboring side-vent-channels; (c) the maximum momentum-transfer reduction effects favor the use of highly-flared side-vent-channels (DV_4 approximately 3.0) in which flaring is done over a relatively small fraction of the channel length (DV_5 approximately 0.3); and (d) the inlet portion of the side-vent-channels should be cut at a negative angle (DV_6 approximately –2° to –14°) relative to the ground in order to further improve the blast-mitigation effects.

4.2.3. SBS Mass Variation along the Pareto Front

Variation of the SBS-mass percent increase (relative to the case of the SBS fitted with a standard V-hull but no side-vent-channels) along the Pareto front is depicted in Figure 15. Examination of this figure shows that, as expected, the design associated with the largest percent reduction in the SBS acceleration corresponds to the largest SBS mass.

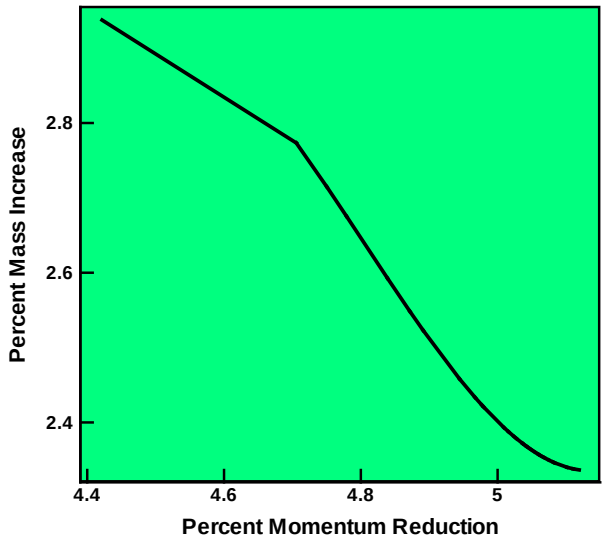

Figure 15. Variation of the SBS-mass percent increase along the Pareto front (relative to the case of the SBS fitted with a standard V-hull but no side-vent-channels).

4.2.4. Statistical Variation of the Optimal Designs

For the most part, the present computational investigation was of a deterministic character. However, due to the granular nature of soil and the statistical aspects of the soil-particle size and shape, computational analyses conducted under nominally identical conditions of the soil density yielded different results. Differences in these results are used in the present section to assess the extent of statistical variability of the optimal SBS designs and their performance, as discussed in the previous section. Specifically, the designs corresponding to points *A* and *B* in Figure 13 are investigated in this section. By carrying out a standard statistical analysis involving the use of the maximum likelihood estimation

method, it was determined that the statistical variability of both optimal designs can be represented using a bi-variate normal distribution function. The results of this analysis are shown, as contour plots, in Figures 16(a)–(b), for the optimal designs *A* and *B*, respectively. Examination of the results displayed in these figures and their subsequent analysis revealed that:

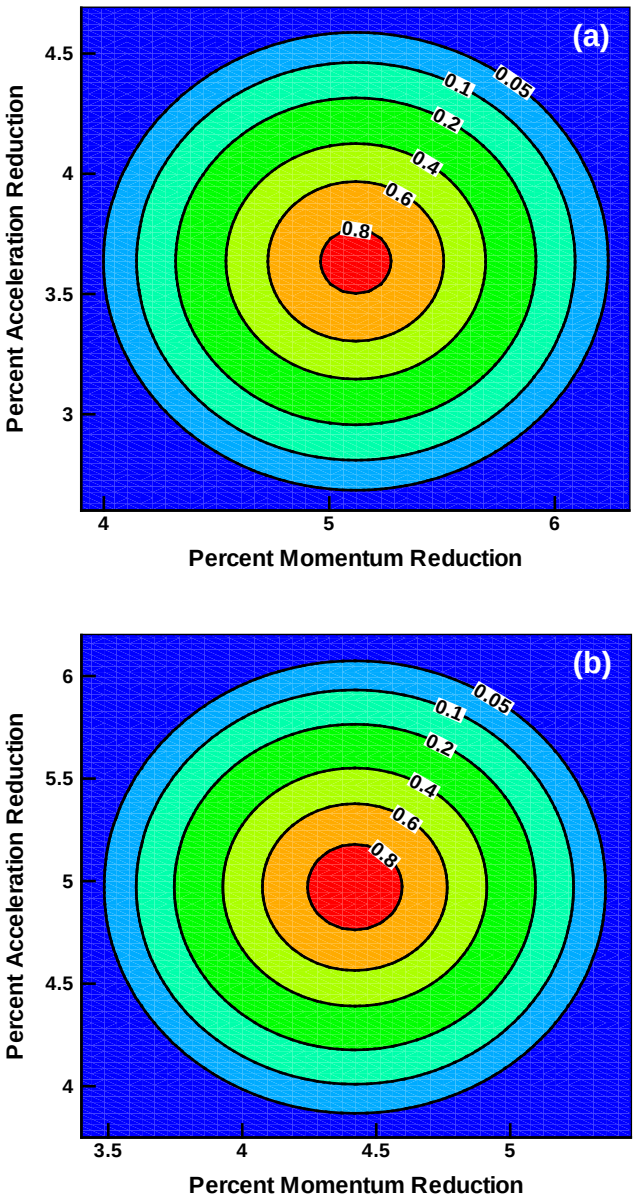

Figure 16. Bi-variate normal-distribution probability density function for: (a) the optimal SBS design *A*, i.e., the design which maximizes the percent momentum reduction; and (b) the optimal SBS design *B*, i.e., the design which maximizes the percent acceleration reduction.

(a) for the optimal design *A*, i.e. for the design which maximizes the percent momentum reduction, the two components of the standard deviation (one associated with the momentum reduction and the other with the acceleration reduction) take on the values of 0.47 and 0.40. This finding suggests that, with a statistical probability of 99.97%, the optimal design *A* offers percent momentum reduction in a 3.71–6.53 range, and percent acceleration reduction in a 2.44–4.84 range; and

(b) for the optimal design *B*, i.e. for the design which maximizes the percent acceleration reduction, the two components of the standard deviation take on the values of 0.39 and 0.46. This finding suggests that, with a statistical probability of 99.97%,

the optimal design *B* offers percent momentum reduction in a 3.25–5.59 range, and percent acceleration reduction in a 3.59–6.35 range.

4.2.5. The Effect of Off-center Mine Position

In all the calculations carried out so far, the landmine was buried (to a constant depth of burial) and centered relative to the footprint of the SBS. In this portion of the work, the effect of the landmine placement at a non-centered position (in the lateral direction) is investigated. An example of the results obtained in this portion of the work is presented in Figure 17. In this figure, a contour plot is shown, with the *x*-axis representing the percent momentum reduction (relative to its counterpart in the case of the SBS fitted with a standard V-hull but no side-vent-channels) and the *y*-axis representing the magnitude of the lateral off-center distance of the mine. On the other hand, the percent acceleration reduction is represented by the contour lines. The plot should be interpreted as a representation of the effect of the mine lateral off-center distance on the trade-off between the two components of the objective function along the Pareto front. Examination of the results displayed in Figure 17 reveals that:

(a) placement of the mine at a laterally non-centered position severely compromises the momentum-reduction capability of the present blast-mitigation solution. Specifically, for the centered position of the mine, the values of the percent momentum reductions along the Pareto front vary between 4.4 and 5.1. On the other hand, at the maximum value of the lateral-offset mine position of 0.5 m, the values of the percent momentum reductions along the Pareto front vary between 1.3 and 2.0;

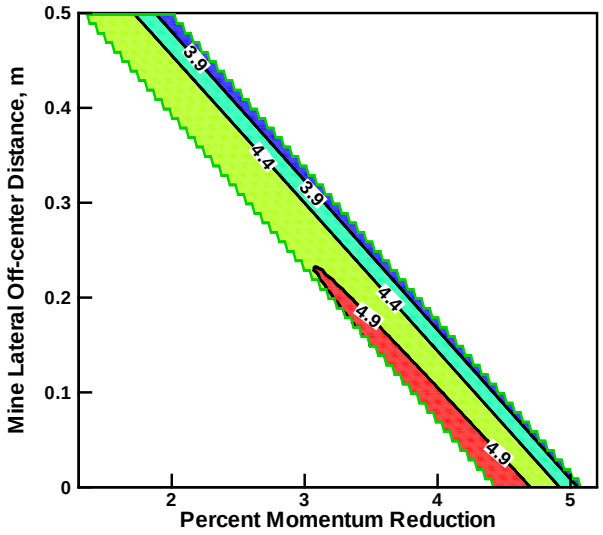

Figure 17. The effect of mine lateral off-center distance (*y*-axis) on the trade-off between percent momentum reduction (*x*-axis) and percent acceleration reduction (contour lines) along the Pareto front.

(b) placement of the mine at a laterally non-centered position also compromises the acceleration-reduction capability of the present blast-mitigation solution, but the effect is not very strong. Specifically, for the centered position of the mine, the values of the percent acceleration reductions along the Pareto front vary between 3.6 and 5.0. On the other hand, at the maximum value of the lateral-offset mine position of 0.5 m, the values of the percent acceleration reductions along the Pareto front vary between 3.3 and 4.8; and

(c) the finding that the percent acceleration reduction is less sensitive to the location of the mine suggests that this blast-mitigation aspect is heavily influenced by the SBS mass. On the other hand, the momentum reduction relies heavily on the ability of the proposed blast-mitigation solution to promote the previously-discussed venting and downward-thrust effects.

5. Bibliography

1. http://www.flickr.com/photos/fisherbray/3574145998/ [Accessed November 18, 2014]
2. M. Grujicic, G. Arakere, H. K. Nallagatla, W. C. Bell, I. Haque, "*Computational Investigation of Blast Survivability and Off-road Performance of an Up-armored High-Mobility Multi-purpose Wheeled Vehicle (HMMWV)*," Journal of Automobile Engineering, 223, 301–325, 2009.
3. M. Grujicic, G. Arakere, W. C. Bell, I. Haque, "*Computational Investigation of the Effect of Up-armoring on Occupant Injury/Fatality Reduction of a Prototypical High-mobility Multi-purpose Wheeled Vehicle Subjected to Mine-blast*," Journal of Automobile Engineering, 223, 903–920, 2009.
4. http://www.flickr.com/photos/trains-n-trucks/3540959347/ [Accessed November 18, 2014]
5. J. Capouellez, K. Drotleff, G. Wolfe, A. Cichosz, F. Helsel, A. Mikaila, J. R. Pickens , R. W. Semelsberger, S. Kerr, E. Wettlaufer, P. Massoud, J. Wood and B. Barringer, "*Optimized Light Tactical Vehicle*," 27th Army Science Conference, No. FP-11, 2010, 1–8.
6. K. Barry and C. Philpot, "*Humvee for Victory*," Car and Driver, Nov. 2011, 22–23.
7. K. Brannen, "*Blast Chimney Shows Promise, Questions Remain*," Defense News, 22 July 2011, http://www.defensenews.com/story.php?i=7166742 [Accessed November 18, 2014]
8. K. Brannen, " *'Chimney' Deflects IEDs,*" Defense News, 1 November 2010, http://www.defensenews.com/story.php?i=4996368 [Accessed November 18, 2014]
9. M. Grujicic, B. P. d'Entremont, J. S. Snipes and R. Gupta, "*A Novel Blast-mitigation Concept for Light Tactical Vehicles*," ARL-TR-6735, Army Research Laboratory 2013.
10. H.P. Zhu, Z.Y. Zhou, R.Y. Yang, A.B. Yu, "*Discrete particle simulation of particulate systems: Theoretical developments*," Chemical Engineering Science, 62, 3378–3396, 2008.
11. H.P. Zhu, Z.Y. Zhou, R.Y. Yang, A.B. Yu, "*Discrete particle simulation of particulate systems: A review of major applications and findings*," Chemical Engineering Science, 63, 5728–5770, 2007.
12. M. Grujicic, R. Yavari, J. S. Snipes, S. Ramaswami, and R. Gupta, "*A Combined Finite-Element/Discrete-Particle Analysis of a Side-Vent-Channel-Based Concept for Improved Blast-Survivability of Light Tactical Vehicles*," ARL-TR-6736, Army Research Laboratory 2013.
13. M. Grujicic, W. C. Bell, "*A Computational Analysis of Survivability of a Pick-Up Truck Subjected to Mine Detonation Loads*," Multidiscipline Modeling in Materials and Structures, 7, 386–423, 2011.
14. M. Grujicic, G. Arakere, X. Xie, M. LaBerge, A. Grujicic, D.W. Wagner, A. Vallejo, "*Design-optimization and material selection for a femoral-fracture fixation-plate implant*," Materials & Design, 31, 3463–3473, 2010.

15. M. Grujicic, W.C. Bell, "*A computational analysis of survivability of a pick-up truck subjected to mine detonation loads*," Multidiscipline Modeling in Materials and Structures 7, 386–423, 2011.

16. D. Gidaspow, *Multiphase Flow and Fluidization*. Academic Press, San Diego, CA, 1994.

17. Y. Tsuji, T. Tanaka, T. Ishida, "*Lagrangian numerical simulation of plug flow of cohesionless particles in a horizontal pipe*," Powder Technology, 71, 239–250, 1992.

18. M. Grujicic, G. Arakere, B. Pandurangan, J. M. Ochterbeck, C-.F. Yen, B. A. Cheeseman, A. P. Reynolds and M. A. Sutton, "*Computational Analysis of Material Flow During Friction Stir Welding of AA5059 Aluminum Alloys*," Journal of Materials Engineering and Performance, 21, 1824–1840, 2012.

19. M. Grujicic, H. Marvi, G. Arakere, W. C. Bell, I. Haque, "*The Effect of Up-armoring the High-Mobility Multi-purpose Wheeled Vehicle (HMMWV) on the Off-road Vehicle Performance*," Multidiscipline Modeling in Materials and Structures, 6, 229–256, 2010.

20. M. Grujicic, V. Sellappan, M. A. Omar, N. Seyr, A. Obieglo, M. Erdmann and J. Holzleitner, "*An Overview of the Polymer-to-Metal Direct-Adhesion Hybrid Technologies for Load-Bearing Automotive Components*", Journal of Materials Processing Technology, 197, 363–373, 2008.

21. ANSYS/AUTODYN, Theory Manual, version 6.1, 2009.

22. M. Grujicic, J. S. Snipes and N. Chandrasekharan, "Computational Investigation of Blast-Wave Mitigation via the Use of Air-vacated Buffers," Journal of Modern Mathematics Frontier, 1, 28–45, 2012.

23. M. Grujicic, J. S. Snipes, N. Chandrasekharan, S. Ramaswami, "*Computational Assessment of the Blast-Mitigation Efficacy of an Air-Vacated Protective-Buffer Concept*," Multidiscipline Modeling in Materials and Structures, 9, 218–242, 2013.

24. M. Grujicic, J. S. Snipes and N. Chandrasekharan, "*Fluid-structure Interaction Computational Analysis of a Piston-Cylinder Based Blast-wave Mitigation Concept*," Multidiscipline Modeling in Materials and Structures, 8, 524–553, 2012.

25. ABAQUS Version 6.10, *User Documentation*, Dassault Systems, 2010.

26. F. H. Walters, L. R. Parker, Jr., S. L. Morgan and S. N. Deming, *Sequential Simplex Optimization. A Technique for Improving Quality and Productivity in Research, Development, and Manufacturing.* CRC Press, Boca Raton, FL, 1991.

27. M. Grujicic, G. Arakere, P. Pisu, B. Ayalew, N. Seyr and M. Erdmann, "*Application of Topology, Size and Shape Optimization Methods in Polymer Metal Hybrid Structural Lightweight Engineering*", Multidiscipline Modeling in Materials and Structures, 4, 305–330, 2008.

28. J. A. Nelder and R. A. Mead, "*A Simplex Method for Function Minimization*," Computer Journal 7, 308–313, 1965.